

Citation format: Mignan, A., L. Danciu and D. Giardini (2015), Reassessment of the Maximum Fault Rupture Length of Strike-Slip Earthquakes and Inference on M_{max} in the Anatolian Peninsula, Turkey. *Seismol. Res. Lett.*, 86 (3), 890-900, doi: 10.1785/0220140252

Reassessment of the Maximum Fault Rupture Length of Strike-Slip Earthquakes and Inference on M_{max} in the Anatolian Peninsula, Turkey

Arnaud Mignan¹, Laurentiu Danciu² and Domenico Giardini¹

¹ Institute of Geophysics, Swiss Federal Institute of Technology (ETH) Zurich,
Sonneneggstrasse 5, CH-8092 Zurich

² Swiss Seismological Service, Swiss Federal Institute of Technology (ETH)
Zurich, Sonneneggstrasse 5, CH-8092 Zurich

Corresponding author: Arnaud Mignan, arnaud.mignan@sed.ethz.ch

INTRODUCTION

Seismic hazard analyses and stress tests for critical infrastructures show limitations in the treatment of extreme events. These extreme events can be great earthquakes and/or their cascading effects, generally not foreseen in risk analysis and management (e.g., Komendantova et al., 2014). For instance, earthquake ruptures are known to potentially propagate over several segments (e.g., Eberhart-Phillips et al., 2003; Fliss et al., 2005). Yet fault segments are still modeled as individual faults in most regional seismic hazard models based on expert opinion and on limited paleoseismic data. Rate anomalies (known as the “bulge”) in the *Uniform California Earthquake*

Rupture Forecast, Version 2 (UCERF2) are in part due to the neglect of possible links between fault segments (Field et al., 2009). Recent catastrophes, such as the 2011 $M_w = 9.0$ Tohoku earthquake and its consequences (e.g., Norio et al., 2011), have demonstrated the need for “a targeted reassessment of the safety margins” of critical infrastructures (ENSREG, 2011).

The present study aims at tackling the issue of potentially unforeseen great earthquakes, (1) by proposing criteria for earthquake rupture cascading over fault segments based on geometrical and physical considerations and (2) by assessing the maximum magnitude (M_{max}) of these ruptures spanning over hundreds of kilometers. Focus is made on strike-slip mechanisms. Different definitions of M_{max} have been proposed based on the assumption that no earthquake is expected above that threshold, such as the maximum observed magnitude, the deterministic “maximum credible” magnitude (Reiter, 1990) and the statistical “maximum possible” magnitude (Kijko and Singh, 2011). It has recently been shown that the predictive power of the statistical approach is rather poor (Zöller et al., 2013). Furthermore, Holschneider et al. (2014) found that it is essentially impossible to infer M_{max} from earthquake catalogues alone. Our method to assess M_{max} is directly related to the deterministic approach, as M_{max} is directly regressed from the length of the fault.

We define a set of simple criteria to assess cascades from individual fault segments by using dynamic stress modeling assumptions (e.g., Kame et al., 2003) and field observations (e.g., Wesnousky, 2006). We apply these criteria to a subset of strike-slip faults in the Anatolian Peninsula, Turkey, as compiled in the 2013 released *European Seismic Hazard Model* (hereafter

ESHM13; Basili et al., 2013). We estimate M_{max} for the resulting cascading events by use of empirical magnitude-length scaling relationships (Stirling et al., 2013 and references therein) taking into account saturation effects at long lengths and other physical constraints (Anderson et al., 1996).

METHOD & DATA

Appraisal of criteria for multi-segment rupture from the dynamic stress modeling literature

Three types of fault segment association can be defined based on geometrical configurations (Fig. 1): (1) bending or rupture propagation along the same fault via segments of potentially different strikes, (2) branching or rupture propagation switching from a segment to a branching segment via a triple junction (in this case, only part of the first segment ruptures), and (3) jumping or propagation from a source to another one, separated in space.

An examination of numerous surface rupture traces of historical strike-slip earthquakes by Wesnousky (2006) showed that ruptures stop propagating (jumping) if the dimension of the fault step Δ is above 3-4 km. For strike-slip faults in Turkey, Barka and Kadinsky-Cade (1988) had already remarked that ruptures generally do not jump step-overs that are wider than 5 km. Dynamic models confirm the importance of the size of the fault step in rupture arrest. Harris and Day (1993) showed that a strike-slip earthquake is unlikely to jump a fault step wider than 5 km, in agreement with field observations. This was confirmed in the case of the 1999 Izmit earthquake, which rupture was stopped by a narrower step-over at its eastern end (Harris et al., 2002). For a rupture to propagate over a wider step, linking structures such as transfer

faults (*en echelon* structures) are necessary, as shown by Harris and Day (1999) in the case of the 1992 Landers earthquake. The most favourable side for bending/branching switches from the extensional to the compressional side as the angle Ψ between the direction of maximum compressive pre-stress and the fault strike becomes shallower. Propagation through bending or branching then depends on the fault geometry, i.e., the inclination φ of a segment with respect to another one (Poliakov et al., 2002; Kame et al., 2003). This has been verified in the case of the 2002 Denali branching earthquake (Bhat et al., 2004).

Based on these two-dimensional geometrical constraints (no depth constraint), we propose the following criteria, which all have to be satisfied for a rupture to propagate along strike from a segment to another one (Fig. 2; see also algorithm in the Appendix):

1. Compatibility of segments: Segments involved in a cascade must have the same mechanism (left- or right-lateral) and the same dip direction (i.e. not antithetic).
2. Maximum distance: The minimum distance Δ between two sources must be lower than 5 km (Harris and Day, 1993; Wesnousky, 2006).
3. Maximum strike difference: The relationship $\psi-\delta \leq \varphi \leq \psi+\delta$ must be respected with φ the angle between two segments (i.e. strike difference), $\psi = \gamma(45-\Psi-180.\text{atan}(\mu_d)/2\pi)$ the optimal angle for rupture (Poliakov et al., 2002; Kame et al., 2003; Bhat et al., 2004), $\Psi > 0$ the angle between the first segment and the direction of maximum compressive stress S_{max} , μ_d the dynamic friction coefficient, $\gamma = 1$ for

right-lateral and $\gamma = -1$ for left-lateral, and $\delta = 30^\circ$ the range of preferred orientation (see Fig. 2 for angle sign convention).

4. Relative position of segments: The rupture can propagate from all or part of a segment to all or part of another segment if the angle between the two subsequent segments remains obtuse (i.e., no backward branching/bending allowed).

Angle notation follows Kame et al. (2003). The term $45-\Psi-180.\text{atan}(\mu_d)/2\pi$ represents the optimum angle once the effect of dynamic friction μ_d is taken into account (Kame et al., 2003). The parameter δ represents the angle range where the shear stress is larger than the frictional resistance, with $\pm\delta = 90^\circ$ the stressed quadrant. The angle Ψ between the fault segment and the direction of maximum compressive stress is defined as $\Psi = \Re/2+45^\circ$ modulo 90° , assuming that variations in the rake \Re represent the variations in the regional stress field orientation. The angle Ψ is defined such that there is no difference between right-lateral and left-lateral mechanisms. It is only the parameter γ that assigns the mechanism and therefore the main orientation of the stressed quadrant. Source orientations are calculated from their tips in disregard of track irregularity. We fix $\mu_d = 0.12$ and $\delta = 30^\circ$ following Kame et al. (2003). The δ value choice is also in agreement with Barka and Kadinsky-Cade (1988), who found that strike-slip ruptures in Turkey do not propagate past bends that have angles greater than about 30° .

Application of these criteria results in a set of cascades, each characterized by a length L_{casc} . The proposed rules are simplifications from the reality and may not represent the full spectrum of possible cascades (see below).

Multi-segment rupture method assumptions and limitations

The proposed method for multi-segment rupture does not consider the case of dip-slip multi-segment rupture. As indicated by Magistrale and Day (1999), it may be misleading to apply results found for strike-slip systems to dip-slip ones since slip direction and strike directions are parallel in the former case and perpendicular in the second. While the same authors found that jumping between thrusts in dynamic stress simulations is limited to $\Delta \leq 2$ km (i.e., different criterion 2), we did not find information regarding the maximum orientation change allowed between two dip-slip segments (i.e., no criterion 3 defined for horizontal propagation of dip-slip ruptures so far). Similarly, criterion 1 enforces that two segments with left- and right-lateral mechanisms cannot rupture together in a same earthquake. Once again, this criterion is based on the fact that no such association has been described in the literature on dynamic stress modeling.

Inclusion of “multifault ruptures” is a new feature of the latest version of the *Uniform California Earthquake Rupture Forecast* (UCERF3; USGS report by Field et al., 2013) compared to the previously published UCERF2 version (Field et al., 2009). Generally, for strike-slip-dominant regimes, our method should satisfy seismic hazard modelers due to its simplicity. Otherwise, the UCERF3 method appears more flexible since it applies for any earthquake mechanism, but at the cost of some subjective choices (e.g., $|\varphi| \leq 60^\circ$ proposed to only prevent large changes in rupture strike, such as right angles or U-turns). Nonetheless, both methods are independent procedures, which can be applied individually when one needs to estimate L_{casc} from which M_{max}

is inferred (this study) or when one needs to model the floating ruptures and their associated rates in seismic hazard analyses (UCERF3).

Rupture velocity (hereafter V_r) is one of the three key parameters to consider in bending/branching scenarios (with the angles Ψ and φ discussed above). Stresses that could initiate rupture on a bend/branch have been shown to significantly increase with crack speed (Poliakov et al., 2002). However, some earthquakes have been observed to propagate very slowly and others very fast (e.g., Bhat et al., 2007 – see also the concept of supershear earthquakes in Rosakis et al., 1999). In our approach, L_{casc} does not depend on V_r , only on the fault network geometry.

Whether a rupture can continue on a larger scale also depends on the history of the stress field in the area (e.g., Poliakov et al., 2002). It has also been recognized that the pre-stress conditions play an important role for a given offset to be breached (Harris and Day, 1999). We assume that the stress field conditions are always favourable for rupture propagation to obtain a conservative estimate of L_{casc} . This assumption avoids including a time-variant component that depends on the earthquake history in the considered region (King et al., 1994).

A last limitation is the sensitivity of the results to the spatial resolution of the fault dataset considered as input for the L_{casc} and M_{max} analysis. This is investigated in detail in the next section.

The ESHM13 database

ESHM13 (Giardini et al., 2013) represents the latest seismic hazard model for the European-Mediterranean region. The model combines the up-

to-date information about earthquakes, active faults and crustal deformation, including the quantification of model and data inherent uncertainties for Europe and Turkey without the limits of national borders. Since the method proposed in the present article is limited to strike-slip mechanisms, we focus our analysis to the Anatolian Peninsula, Turkey, where strike-slip structures are predominant and have the potential to rupture over great distances.

We use the fault sources as compiled in ESHM13 and described in the European Database of Seismogenic Faults (available at <http://diss.rm.ingv.it/share-edsf/>, last assessed September 2014). The seismically active faults, as defined by Basili et al. (2010), represent a composite structure that consists of multiple single mapped faults. By this definition, the size of a composite seismogenic source spans a larger area than the one of the largest observed earthquake due to high uncertainties on the end-points of the defined segments. The end-points were defined either at the end of an adjacent identified fault rupture or at a significant structural change (Haller and Basili, 2011).

Figure 3 shows a map of the region including the fault mechanisms derived from the source rake \mathfrak{R} (see inset for rake/mechanism convention in ESHM13). We only consider strike-slip faults for our analysis, with $\mathfrak{R} \leq 45^\circ$ or $\mathfrak{R} \geq 315^\circ$ for left-lateral faults and $135^\circ \leq \mathfrak{R} \leq 225^\circ$ for right-lateral faults. Since ESHM13 only provides minimum and maximum values of the rake, we use $\mathfrak{R} = (\mathfrak{R}_{min} + \mathfrak{R}_{max})/2$. Arithmetic mean values are also used for other ESHM13 parameters (strike, dip and slip rate).

Assessment of M_{max} considering individual fault segment lengths or cascade lengths

M_{max} is commonly estimated from the length L of individual fault segments. We first investigate the scaling relationships listed in Table 1 (Wells and Coppersmith, 1994; Mai and Beroza, 2000; Hanks and Bakun, 2002; Leonard, 2010; Wesnousky, 2008), used in ESHM13 and/or recommended by Stirling et al. (2013) for the case of “plate boundary crustal, fast plate boundary faults, strike-slip dominated” (their tectonic regime A11). Figure 4 compares these relationships to the ESHM13 data here defined by M_{max} , the total length L_{tot} and the effective length L_{eff} . L_{tot} spans the entire composite source, geographically defined (i.e., the “trace length in map view” definition of Kim and Sanderson, 2005). It is not directly linked to the assigned ESHM13 M_{max} but represents possible extensions of the individual fault ruptures, due to uncertainty in their location – hence the use of a potentially lower L_{eff} to account for low slip rates, historical observations, etc.. In our study, we only use a conservative $L_{casc} = L_{tot}$ while correcting for slip rates at a later stage. In ESHM13, the minimum, median and maximum lengths of fault segments are 17 km, 50 km and 360 km, respectively (Fig. 4a). For the longest length, the corresponding M_{max} equals 8.1 in ESHM13 (composite source case).

In the case of rupture cascades, the resulting rupture length L_{casc} can easily reach several hundreds of kilometres, which in turn exceeds the calibration range of the magnitude-length scaling equations. In this view, we dismiss the equations proposed by Mai and Beroza (2000) (estimated $L_{max} = 180$ km) and by Leonard (2010) (estimated $L_{max} = 50$ km for strike-slip

ruptures). We also do not use the relationship by Wells and Coppersmith (1994) since Hanks and Beroza (2002) include their dataset while adding five more strike-slip ruptures above 200 km long. We therefore use the two remaining relationships, i.e. Hanks and Bakun (2002) and Wesnousky (2008) ($L_{max} \sim 430$ km in both cases), that we prolong to over 1,000 km, as well as the scaling equation of Anderson et al. (1996) (Table 1, $L_{max} = 470$ km), in which the slip rate (s) is an additional physical constraint on M_{max} . These three relationships are considered to account for epistemic uncertainties.

RESULTS

Strike-slip cascades in the Anatolian Peninsula

For the dataset considered consisting of 217 single fault segments, the algorithm for multi-segment rupture (see Appendix) produces a total of 272 cascades (including some redundancies). Figure 5a shows an example of cascade on the North Anatolian Fault (NAF), which is composed of seven ESHM13 fault segments, complete or partial. Figure 5b shows the longest rupture cascades possible in different parts of the Anatolian Peninsula based on the data and method employed (with $\Delta = 5$ km).

It should be noted that these results are sensitive to the definition of the fault network trace and to the values of Δ and δ . While the defined mean orientation of a fault segment is likely accurate, the gap between different segments depends on the spatial resolution of the fault mapping, indicating the importance of improved fault mapping in seismic hazard studies, especially considering the link between the different structures in three dimensions (e.g., slip-partitioning and complex *decollements*) (e.g., Choi et

al., 2012). Ambraseys (1970) noted that the Anatolian fault zone appears at a small scale as a continuous structure except for the step near Niksar (Fig. 5b). This step explains why no rupture cascades along the full NAF structure when using the ESHM13 database and $\Delta = 5$ km. However *en echelon* structures link the two fault segments at a larger scale, which suggests possible jumping between the eastern and western sides of the NAF when refined information is used.

While we consider that the values $\Delta = 5$ km and $\delta = 30^\circ$ fixed in the criteria defined above are reliable physical constraints, verified in both dynamic models (Harris and Day, 1993; Kame et al., 2003; Harris et al., 2002) and in the field (Wesnousky, 2006; Barka and Kadinsky-Cade, 1988), Δ may need some adjustment in order to take into account obvious inconsistencies in the fault input dataset. This is investigated in the next section with the mapping of M_{max} .

It should be added that the rupture cascades generated could not be compared to historical complex ruptures, which are already defined as ESHM13 sources (e.g., 1939 Ercincan, 1943 Ladik and 1999 Izmit earthquakes, which all present bends – Ambraseys, 1970; Harris et al., 2002). In other words, all the cascades generated here are potential ruptures that have not yet been observed.

Reassessment of M_{max} considering rupture cascade lengths in the Anatolian Peninsula

Figure 6a shows the distribution of rupture cascade lengths L_{casc} with minimum, median and maximum lengths of 33 km, 254 km and 853 km,

respectively for the “standard” $\Delta = 5$ km. For an increased $\Delta = 10$ km, the median and maximum lengths increase to 436 km and 1480 km, respectively. It means – following the proposed method – that events could rupture over more than twice the length of the longest fault defined in ESHM13 when considering the standard input parameters ($\Delta = 5$ km, $\delta = 30^\circ$) but that they could rupture over more than four times the ESHM13 maximum length if a more conservative Δ value of 10 km is used.

Figure 6b shows M_{max} values assessed from the scaling relationships of Hanks and Bakun (2002), Wesnousky (2008) and Anderson et al. (1996). For the latter, the slip rate of a cascade is defined as the average of the slip rates of the connected ESHM13 segments. We find that the Anderson et al. (1996) values (points) are comprised between the Hanks and Bakun (2002) and Wesnousky (2008) estimates (curves). For $L_{max}(\Delta = 5 \text{ km}) = 853 \text{ km}$, $M_{max}(\text{HB02}) = 8.65 \pm 0.05$, $M_{max}(\text{W08}) = 8.11 \pm 0.24$ and $M_{max}(\text{A96}) = 8.30 \pm 0.29$. For $L_{max}(\Delta = 10 \text{ km}) = 1480 \text{ km}$, $M_{max}(\text{HB02}) = 8.97 \pm 0.04$, $M_{max}(\text{W08}) = 8.32 \pm 0.24$ and $M_{max}(\text{A96}) = 8.53 \pm 0.29$. The range of possible values for a given L_{casc} indicates a large epistemic uncertainty, which can be partially due to the use of the scaling relationships beyond their calibration range. Reduction of these uncertainties is out of the scope of this study.

Figure 7 shows M_{max} maps of the strike-slip faults in the Anatolian Peninsula for ESHM13 segments (Fig. 7a) and for multi-segment cascades with standard $\Delta = 5$ km (Fig. 7b) and increased $\Delta = 10$ km (Fig. 7c). M_{max} is computed for all maps using the relationship of Anderson et al. (1996). As already discussed earlier, an earthquake cannot rupture all along the NAF when using the standard $\Delta = 5$ km (Fig. 5b; Fig. 7b). However plate

boundaries, such as the NAF (e.g., Ambraseys, 1970), are continuous structures that shall be able to rupture in one event. This is here obtained by using a more conservative $\Delta = 10$ km (Fig. 7c). A correction to Δ shall be applied whenever the spatial resolution of the fault trace data is too low relative to the standard $\Delta = 5$ km.

We find that M_{max} is increased locally from about 0.5 to 1.5 units along the NAF and the East Anatolian Fault (EAF). A number of other faults show an increase from about 0.5 to 1.0 (Figs. 7a-7c). Note that these results are subject to epistemic uncertainties (see Fig. 6). With longer ruptures being characterized by greater slip and a wider shaking spatial footprint, our results suggest a change in hazard in the Anatolian Peninsula once cascades are considered. This will be investigated in detail in a future study.

In ESHM13, the area source M_{max} is assigned as the largest value between the historical observations and largest maximum magnitude as estimated from fault sources, plus an increment of 0.2 corresponding to the reported magnitude error on the earthquake catalogue (Meletti et al., 2009). For the NAF area source, the largest value $M_{max} = 8.6$ has a weight of only 0.1 (Basili et al., 2010). A similar M_{max} is obtained from the Anderson et al. (1996) relationship, while lower and higher values are also possible depending on the selected scaling relationship (range of values given above). It is well known that the M_{max} of strike-slip events are unlikely to reach M_w 9 values since great strike-slip ruptures scale with length L and not area L^2 (e.g., Romanowicz and Ruff, 2002). The 2012 equatorial Indian Ocean earthquakes of M_w 8.6 (mainshock) and 8.2 (aftershock) were two of the largest strike-slip earthquakes ever recorded (Duputel et al., 2012). In that view, extrapolation of

the Hanks and Bakun (2002) relationship beyond its calibration range (with $M_{max} \sim 9$) becomes questionable.

IMPLICATIONS FOR STRESS TESTS & HAZARD ASSESSMENT

A stress test is defined as a targeted assessment of the safety margins of a given critical infrastructure. This assessment consists in particular in the evaluation of the response of the critical infrastructure when facing a set of extreme situations (ENSREG, 2011). In this context, we are interested in generating the “worst” earthquake magnitude that is physically possible. Seismic hazard analyses must also define the largest earthquake possible within a specified source zone or known fault.

The proposed multi-segment rupture approach – by generating physically constrained cascades linking individual fault segments – provides refined values of M_{max} . It can be used in deterministic hazard applications, for example for stress test what-if scenarios, by converting the longest modeled cascade rupture L_{casc} into an M_{max} using empirical magnitude-length scaling relationships. In addition, by applying the algorithm presented in the Appendix, a cascade dataset is generated that can serve as input for probabilistic seismic hazard modeling. Occurrence rates could then be estimated by using the rules already established for composite sources (i.e., using Gutenberg-Richter or characteristic earthquake models, conservation of total seismic moment rate, etc.).

APPENDIX: Multi-Segment Rupture Algorithm

An algorithm is proposed to generate cascades based on the four defined criteria for multi-segment rupture. It is an iterative procedure for searching, identifying and linking individual sources into longer fault structures of length L_{casc} :

1. Input: Select all strike-slip individual fault segments from a fault source database defined by rake $\Re \leq 45^\circ$ or $\Re \geq 315^\circ$ for left-lateral faults and $135^\circ \leq \Re \leq 225^\circ$ for right-lateral faults. Fix increment $i = 0$ and define the set S_0 composed of the n_0 selected segments.

2. Cascade definition loop: For each segment $1 \leq j \leq n_i$ of set S_i :

2.1 Maximum distance (jumping): Define a buffer $\Delta = 5$ km wide (or wider – see text for details) from segment j . Find all segments $k_{tmp} \neq j$ of set S_0 with at least one coordinate point within the buffer zone and with the same mechanism (right-lateral or left-lateral) and dip direction (positive or negative).

2.2 Maximum strike difference (bending/branching): Calculate $\Psi = \Re_j/2+45^\circ$ modulo 90° and $\psi = \gamma_j(45-\Psi-180.\text{atan}(\mu_d)/2\pi)$ with $\gamma_j = 1$ or -1 if segment j is right- or left-lateral, respectively and $\mu_d = 0.12$. Find all segments $k \in k_{tmp}$ which verify $\psi-\delta \leq \varphi_{jk} \leq \psi+\delta$ with $\delta = 30^\circ$ and φ_{jk} the difference between the strikes of segments j and k (see Fig. 2 for angle sign convention).

2.3 Relative position of segments (Fig. A1): For each segment k , find the 2 nearest anchor points linking segments j and k , each located on segment j and k , respectively. Define the sub-segments j_A , j_B , k_A and k_B defined from the tips of the original segments and the 2 anchor points. Of all possible sub-segment combinations $\{j_A - k_A, j_A - k_B, j_B - k_A, j_B - k_B\}$, keep only the combinations with obtuse angle (i.e. no backward propagation). If more than one combination remains, save only the longest cascade into the

cascade set S_{i+1} and define the cascade rake and strike as the arithmetic mean of the rakes and strikes of the 2 sub-segments.

3. Cascade growth loop: Fix $i = i+1$ and repeat step 2 until the number of cascades in S_i is $n_i = 0$ (Fig. A2) or tends to a constant maximum cascade length L_{max} (Fig. A3). Save all cascades of set S_i into the final cascade set S_{casc} .

In the first iteration $i = 0$, both segments j and k are individual fault segments from input set S_0 . In subsequent iterations $i \geq 1$, the input segments j are the cascades defined in the previous iteration, such that any cascade in set S_i is composed of $i+1$ individual segments (or sub-segments). For the case of the Anatolian Peninsula ESHM13 fault segments with $\Delta = 5$ km, the algorithm stopped at iteration $i = 9$ indicating that the longest cascades were composed of 10 ESHM13 segments, complete or partial, in set S_9 (Fig. A2). Depending on the fault data configuration, some redundancies may occur (i.e. non-unique sub-segment associations yielding a same cascade path). Although the number of cascades dropped to $n_{10} = 0$ in the present analysis for $\Delta = 5$ km, it is possible that redundant cascades may lead to $n_{\infty} > 0$. In such a case, step 3 of the algorithm includes a test for maximum length L_{max} stability combined to a maximum number of possible iterations. This is for example the case when using $\Delta = 10$ km, for which stability is obtained at iteration $i = 11$ (Fig. A3). By construction, all the cascades generated have tips which match with existing tips of different individual segments defined in ESHM13.

ACKNOWLEDGMENTS

We are thankful to the Editor and two anonymous reviewers for their helpful comments. The research leading to these results has been supported by the *Harmonized approach to stress tests for critical infrastructures against natural hazards* (STREST) project, funded by the European Community's Seventh Framework Programme [FP7/2007-2013] under Grant Agreement No. 603389 and by the Swiss Competence Center for Energy Research – Supply of Electricity (SCCER-SoE).

REFERENCES

- Ambraseys, N. N. (1970), Some characteristic features of the Anatolian Fault Zone, *Tectonophysics*, 9, 143-165
- Anderson, J. G., S. G. Wesnousky and M. W. Stirling (1996), Earthquake Size as a Function of Fault Slip Rate, *Bull. Seismol. Soc. Am.*, 86, 683-690
- Barka, A. A. and K. Kadinsky-Cade (1988), Strike-slip fault geometry in Turkey and its influence on earthquake activity, *Tectonophysics*, 7, 663-684
- Basili R., et al. (2013), The European Database of Seismogenic Faults (EDSF) compiled in the framework of the Project SHARE, doi:10.6092/INGV.IT-SHARE-EDSF, available at: <http://diss.rm.ingv.it/share-edsf/> (last assessed September 2014)
- Bhat, H. S., R. Dmowska, J. R. Rice and N. Kame (2004), Dynamic Slip Transfer from the Denali to Totschunda Faults, Alaska: Testing Theory for Fault Branching, *Bull. Seismol. Soc. Am.*, 94, S202-S213
- Bhat, H. S., M. Olives, R. Dmowska and J. R. Rice (2007), Role of fault branches in earthquake rupture dynamics, *J. Geophys. Res.*, 112, B11309, doi: 10.1029/2007JB005027

Choi, J.-H., K. Jin, D. Enkhbayar, B. Davvasambuu, A. Bayasgalan and Y.-S. Kim (2012), Rupture propagation inferred from damage patterns, slip distribution, and segmentation of the 1957 M_w 8.1 Gobi-Altay earthquake rupture along the Bogd fault, Mongolia, *J. Geophys. Res.*, 117, B12401, doi: 10.1029/2011JB008676

Duputel, Z., H. Kanamori, V. C. Tsai, L. Rivera, L. Meng, J. P. Ampuero and J. M. Stock (2012), The 2012 Sumatra great earthquake sequence, *Earth Planet. Sci. Lett.*, 351, 247-257, doi: 10.1016/j.epsl.2012.07.017

Eberhart-Phillips, D., et al. (2003), The 2002 Denali Fault Earthquake, Alaska: A Large Magnitude, Slip-Partitioned Event, *Science*, 300, 1113-1118, doi: 10.1126/science.1082703

ENSREG (European Nuclear Safety Regulators Group) (2011), Declaration of ENSREG, Annex 1, EU “Stress test” specifications, Brussels 31.05.2011, available at <http://www.ensreg.eu/node/289> (last assessed September 2014)

Field, E. H., et al. (2009), Uniform California Earthquake Rupture Forecast, Version 2 (UCERF 2), *Bull. Seismol. Soc. Am.*, 99, 2053-2107, doi: 10.1785/0120080049

Field, E. H., et al. (2013), Uniform California earthquake rupture forecast, version 3 (UCERF3) – The time-independent model, U.S. Geological Survey Open-File Report 2013-1165, 97 pp., California Geological Survey Special Report 228, and Southern California Earthquake Center Publication 1792, <http://pubs.usgs.gov/of/2013/1165/> (last assessed September 2014)

- Fliss, S., H. S. Bhat, R. Dmowska and J. R. Rice (2005), Fault branching and rupture directivity, *J. Geophys. Res.*, 110, B06312, doi: 10.1029/2004JB003368
- Giardini, D., et al. (2013), Seismic Hazard Harmonization in Europe (SHARE): Online Data Resource, doi: 10.12686/SED-00000001-SHARE
- Haller, K. M. and R. Basili (2011), Developing Seismogenic Source Models Based on Geologic Fault Data, *Seismol. Res. Lett.*, 82, 519-525, doi: 10.1785/gssrl.82.4.519v
- Hanks, T. C. and W. H. Bakun (2002), A Bilinear Source-Scaling Model for $M_{log A}$ Observations of Continental Earthquakes, *Bull. Seismol. Soc. Am.*, 92, 1841-1846
- Harris, R. A. and S. M. Day (1993), Dynamics of Fault Interaction: Parallel Strike-Slip Faults, *J. Geophys. Res.*, 98, 4461-4472
- Harris, R. A. and S. M. Day (1999), Dynamic 3D simulations of earthquakes on en echelon faults, *Geophys. Res. Lett.*, 26, 2089-2092
- Harris, R. A., J. F. Dolan, R. Hartleb and S. M. Day (2002), The 1999 Izmit, Turkey, Earthquake: A 3D Dynamic Stress Transfer Model of Intraearthquake Triggering, *Bull. Seismol. Soc. Am.*, 92, 245-255
- Heaton, T. H. and H. Kanamori (1984), Seismic potential associated with subduction in the Northwestern United States, *Bull. Seismol. Soc. Am.*, 74, 933-941
- Holschneider, M., G. Zöller, R. Clemens and D. Schorlemmer (2014), Can we test for the maximum possible earthquake magnitude?, *J. Geophys. Res.*, 119, 2019-2028, doi: 10.1002/2013JB010319

- Kame, N., J. R. Rice and R. Dmowska (2003), Effects of pre-stress state and rupture velocity on dynamic fault branching, *J. Geophys. Res.*, 108, 2265, doi: 10.1029/2002JB002189
- Kijko, A. and M. Singh (2011), Statistical Tools for Maximum Possible Earthquake Magnitude Estimation, *Acta Geophysica*, 59, 674-700, doi: 10.2478/s11600-011-0012-6
- Kim, Y.-S. and D. J. Sanderson (2005), The relationship between displacement and length of faults: a review, *Earth-Science Reviews*, 68, 317-334
- King, G. C. P., R. S. Stein and J. Lin (1994), Static Stress Changes and the Triggering of Earthquakes, *Bull. Seismol. Soc. Am.*, 84, 935-953
- Komendantova, N., R. Mrzyglocki, A. Mignan, B. Khazai, F. Wenzel, A. Patt and K. Fleming (2014), Multi-hazard and multi-risk decision-support tools as a part of participatory risk governance: Feedback from civil protection stakeholders, *International Journal of Disaster Risk Reduction*, 8, 50-67, doi: 10.1016/j.ijdrr.2013.12.006
- Leonard, M. (2010), Earthquake Fault Scaling: Self-Consistent Relating of Rupture Length, Width, Average Displacement, and Moment Release, *Bull. Seismol. Soc. Am.*, 100, 1971-1988, doi: 10.1785/0120090189
- Magistrale, H. and S. Day (1999), 3D Simulations of Multi-Segment Thrust Fault Rupture, *Geophys. Res. Lett.*, 26, 2093-2096
- Mai, P. M. and G. C. Beroza (2000), Source Scaling Properties from Finite-Fault-Rupture Models, *Bull. Seismol. Soc. Am.*, 90, 604-615

- Meletti, C., V. D'Amico and F. Martinelli (2009), Homogeneous determination of the maximum magnitude, SHARE project, D3.1 deliverable, available at http://www.earth-prints.org/bitstream/2122/6530/1/D3.3_SHARE.pdf
- Norio, O., T. Ye, Y. Kajitani, P. Shi and H. Tatano (2011), The 2011 Eastern Japan Great Earthquake Disaster: Overview and Comments, Int. J. Disaster Risk Sci., 2, 34-42
- Poliakov, A. N. B., R. Dmowska and J. R. Rice (2002), Dynamic shear rupture interaction with fault bends and off-axis secondary faulting, J. Geophys. Res., 107, 2295
- Reiter, L. (1990), Earthquake Hazard Analysis: Issues and Insights, Columbia University Press, 254 pp.
- Romanowicz, B. and L. J. Ruff (2002), On moment-length scaling of large strike slip earthquakes and the strength of faults, Geophys. Res. Lett., 29, 1604, doi: 10.1029/2001GL014479
- Rosakis, A. J., O. Samudrala and D. Coker (1999), Cracks Faster than the Shear Wave Speed, Science, 284, 1337-1340, doi: 10.1126/science.284.5418.1337
- Stirling, M., T. Goded, K. Berryman and N. Litchfield (2013), Selection of Earthquake Scaling Relationships for Seismic-Hazard Analysis, Bull. Seismol. Soc. Am., 103, 2993-3011, doi: 10.1785/0120130052
- Wells, D. L. and K. J. Coppersmith (1994), New Empirical Relationships among Magnitude, Rupture Length, Rupture Width, Rupture Area, and Surface Displacement, Bull. Seismol. Soc. Am., 84, 974-1002
- Wesnousky, S. G. (2006), Predicting the endpoints of earthquake ruptures, Nature, 444, 358-360, doi: 10.1038/nature05275

Wesnousky, S. G. (2008), Displacement and Geometrical Characteristics of Earthquake Surface Ruptures: Issues and Implications for Seismic-Hazard Analysis and the Process of Earthquake Rupture, *Bull. Seismol. Soc. Am.*, 98, 1609-1632, doi: 10.1785/0120070111

Zöller, G., M. Holschneider and S. Hainzl (2013), The Maximum Earthquake Magnitude in a Time Horizon: Theory and Case Studies, *Bull. Seismol. Soc. Am.*, 103, 860-875, doi: 10.1785/0120120013

Tables:

Table 1: Standard $M_w - \log(L)$ scaling relationships with moment magnitude M_w and length L in km. 1: Used in ESHM13; 2: Recommended by Stirling et al. (2013); 3: Considered in the present study for long strike-slip ruptures, including the role of slip rate s (in mm/yr) in one case.

Reference	Relationship*	Parameters (\pm standard error)	1	2	3
Wells and Coppersmith (1994)	$M_w = a \log(L) + b$	$a = 1.12 (\pm 0.13); b = 5.16 (\pm 0.08)$	✓		
Mai and Beroza (2000)	$M_w = 0.67 (\log(L) - a) / b + 7 - 10.7$	$a = -5.15 (\pm 1.11); b = 0.36 (\pm 0.06)$	✓		
Hanks and Bakun (2002)	$M_w = a \log(A) + b$	{ $A \leq 537 \text{ km}^2$: $a = 1; b = 3.98 (\pm 0.03)$ }; { $A > 537 \text{ km}^2$: $a = 4/3; b = 3.07 (\pm 0.04)$ }	✓	✓	✓
Leonard (2010)	$M_w = a \log(L) + b$	$a = 1.67; b = 4.24$	✓	✓	
Wesnousky (2008)	$M_w = a \log(L) + b$	$a = 0.87; b = 5.56; M_w \pm 0.24$		✓	✓
Anderson et al. (1996)	$M_w = A + B \log L - C \log s$	$A = 5.12 (\pm 0.12); B = 1.16 (\pm 0.07); C = 0.20 (\pm 0.04)$			✓

* For strike-slip mechanisms when discriminated in a study. For area-magnitude relationships, $A = WL$ with width $W = 18 \text{ km}$ (arithmetic mean of ESHM13 strike-slip composite sources in Turkey).

Figures:

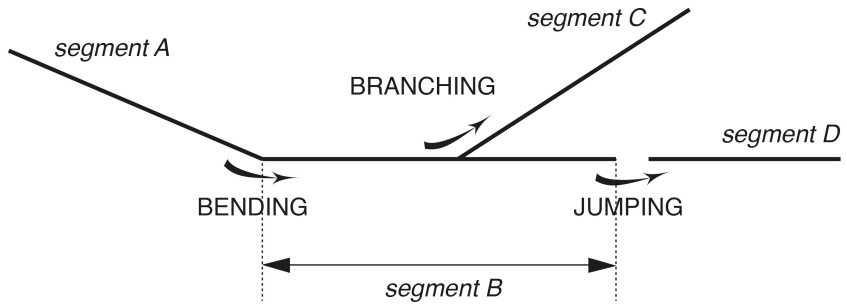


Figure 1: Different types of fault segment association (bending, branching and jumping).

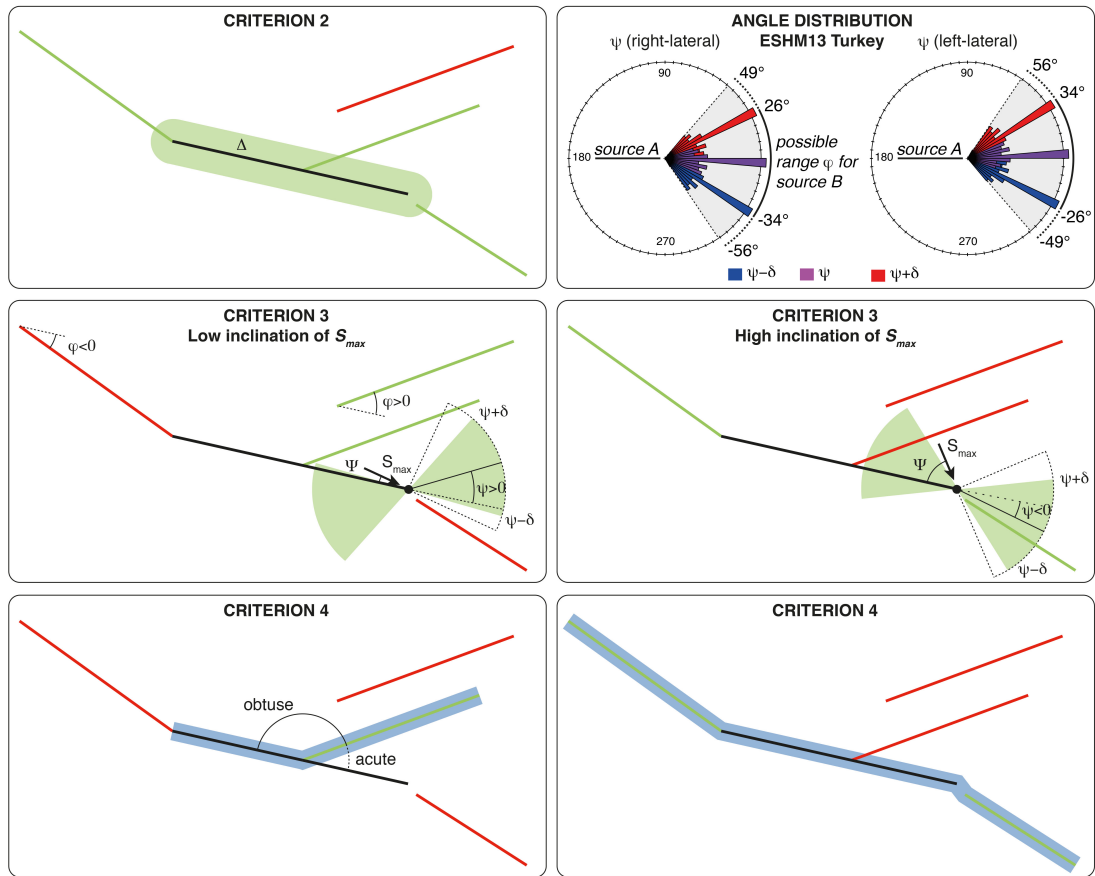


Figure 2: Criteria 2 to 4 defined for multi-segment rupture (shown in map view). Segments in green verify the criterion while segments in red do not. Other illustrations of criterion 3 can be found in Poliakov et al. (2002) and Kame et al. (2003). The blue bands represent the possible rupture cascades

for the proposed geometrical and regional stress configurations. Note the significance of the regional stress field orientation represented here by two different inclinations of the maximum compressive stress S_{max} .

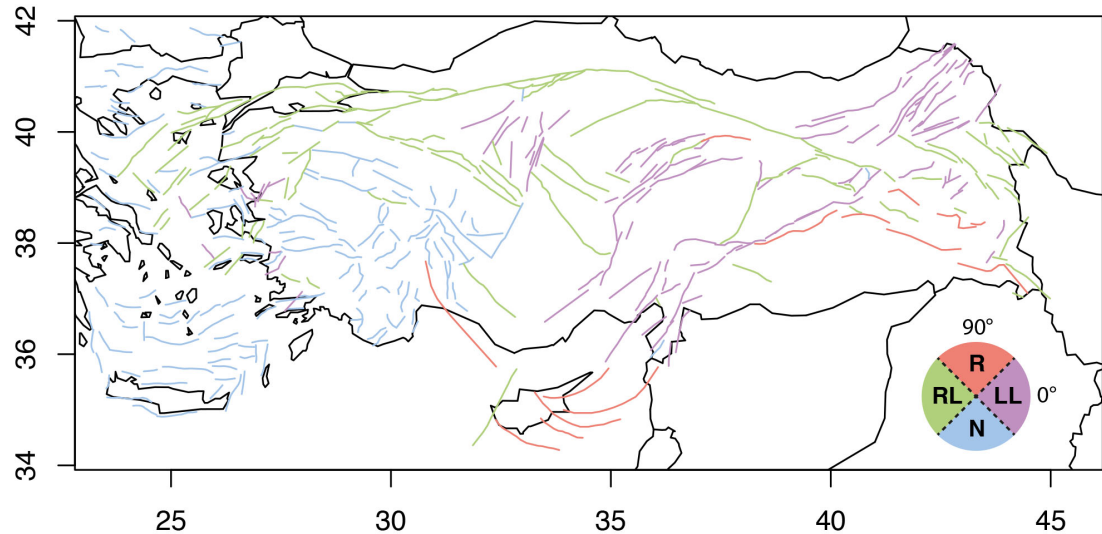


Figure 3: Fault map of the Anatolian Peninsula, as defined in ESHM13 (Basili et al., 2013). Convention between rakes \mathfrak{R} and mechanisms is given in the lower right corner of the map.

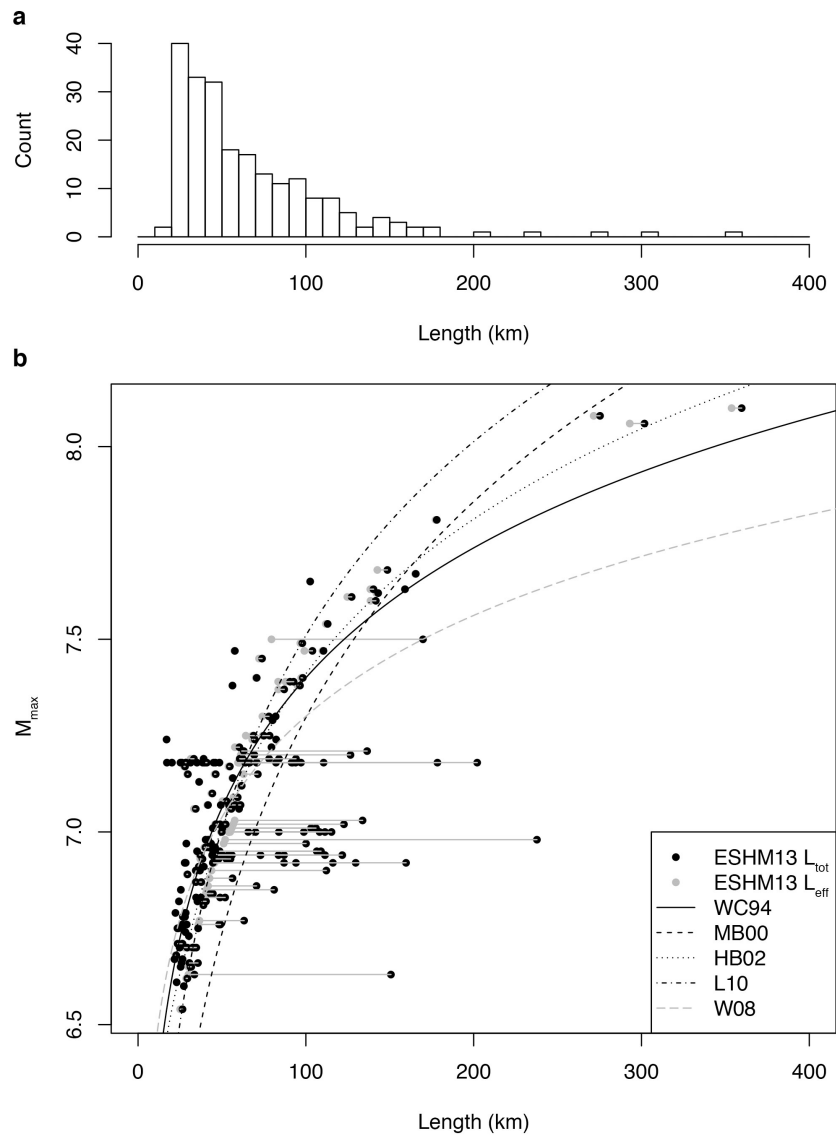


Figure 4: ESHM13 length – M_{max} data for strike-slip fault segments in the Anatolian Peninsula; a. Composite source length (L_{tot}) distribution; b. Standard M – $\log(L)$ scaling relationships compared to ESHM13 data. WC94: Wells and Coppersmith (1994), MB00: Mai and Beroza (2000), HB02: Hanks and Bakun (2002), L10: Leonard (2010) and W08: Wesnousky (2008) (see Table 1).

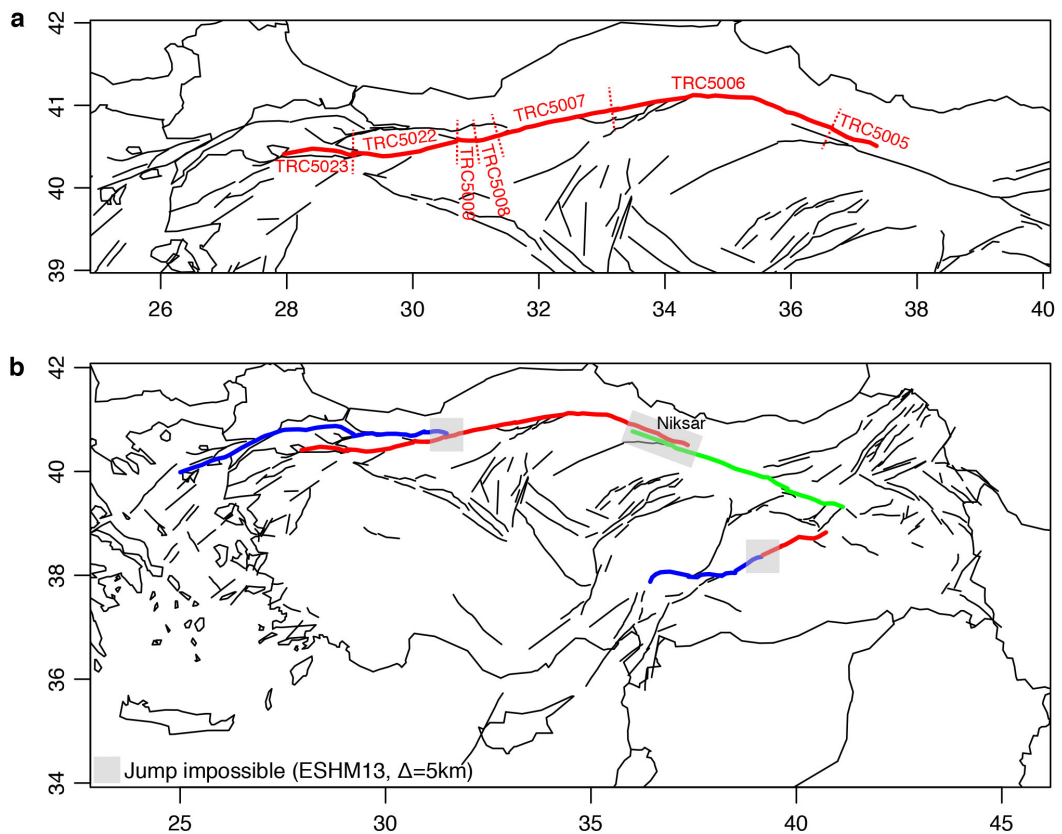


Figure 5: Examples of generated strike-slip cascades in the Anatolian Peninsula; a. Example of multi-segment rupture on the North Anatolian Fault composed of seven ESHM13 individual segments; b. The longest cascades possible in different parts of Turkey, constrained by the ESHM13 fault network representation and the defined rules for multi-segment rupture (here with standard $\Delta = 5$ km). Each colored fault rupture represents one cascade.

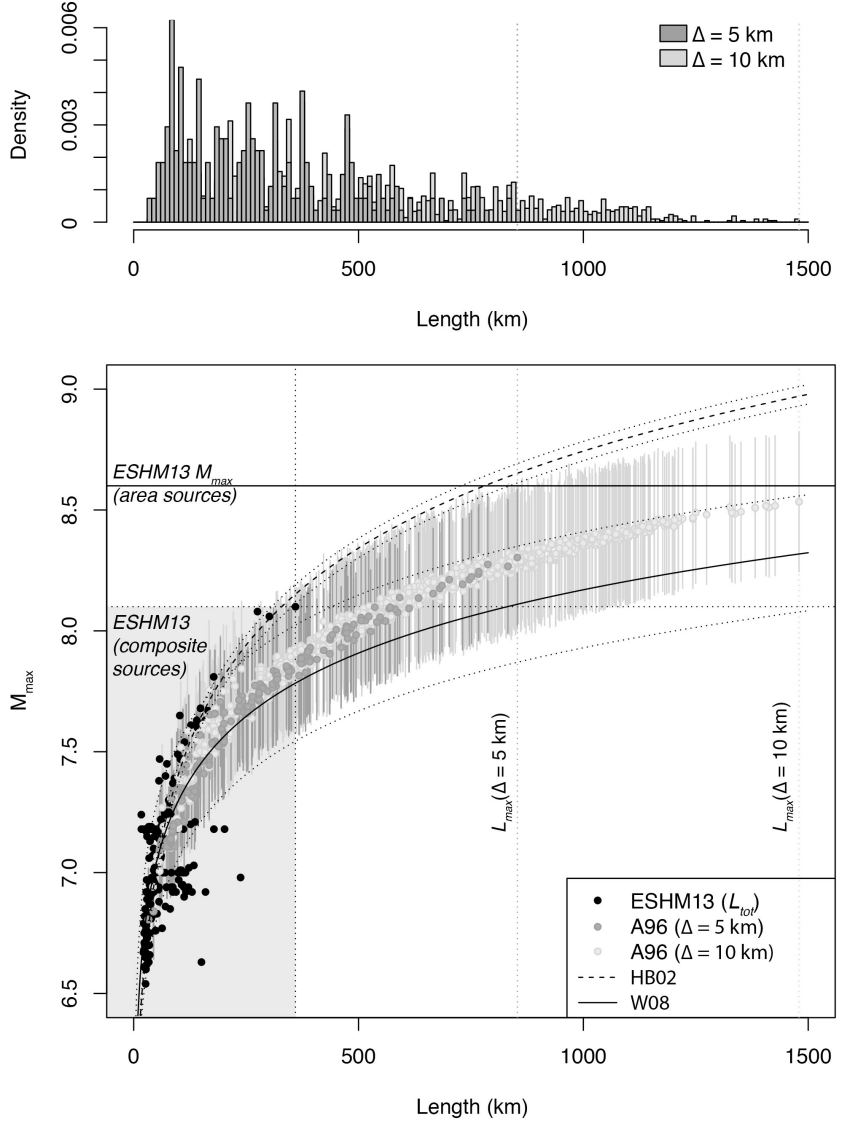


Figure 6: Length – M_{max} scaling for strike-slip cascades in the Anatolian Peninsula; a. Rupture cascade length distribution for two values of Δ ; b. M_{max} derived from rupture cascade lengths L_{casc} using three different magnitude-length scaling relationships: A96: Anderson et al. (1996), HB02: Hanks and Bakun (2002) and W08: Wesnousky (2008) (see Table 1). Error bars represent ± 1 -sigma.

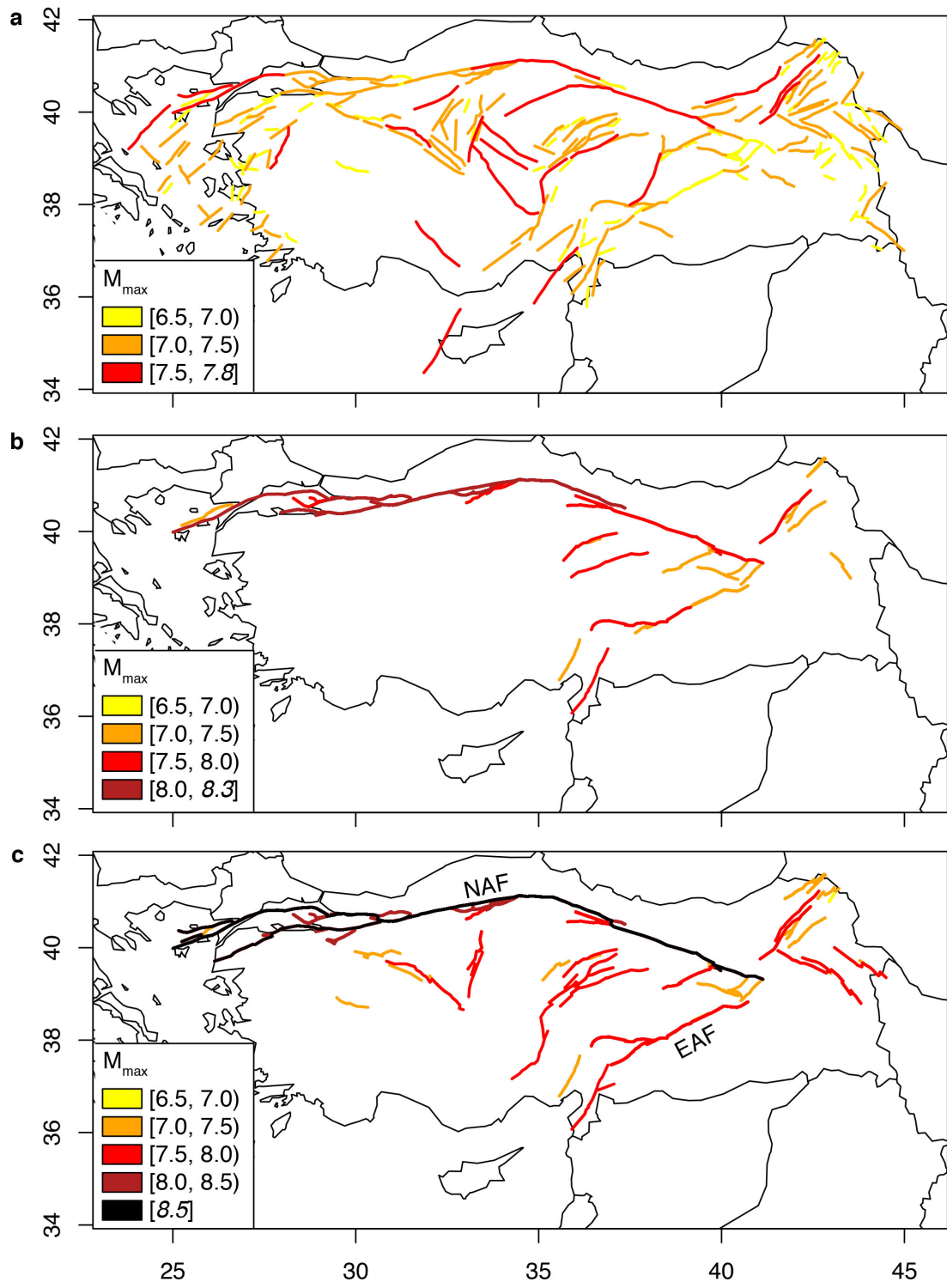


Figure 7: M_{max} maps for strike-slip faults in the Anatolian Peninsula, computed from the Anderson et al. (1996) relationship; a. ESHM13 segments; b. Multi-segment cascades with $\Delta = 5$ km; c. Multi-segment cascades with $\Delta = 10$ km. Value in italics is the maximum computed.

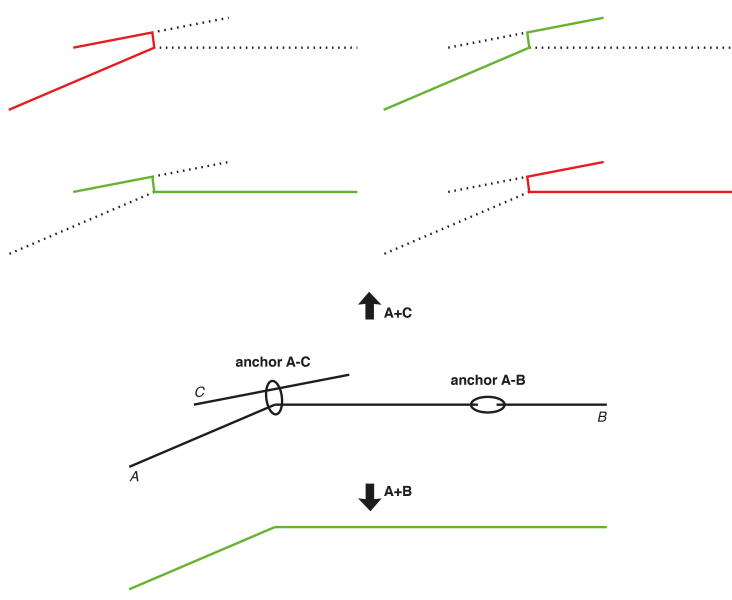


Figure A1: Illustration of step 2.3 of the algorithm. Cascades in green are valid (obtuse angle between segments) while cascades in red are not (acute angle between segments).

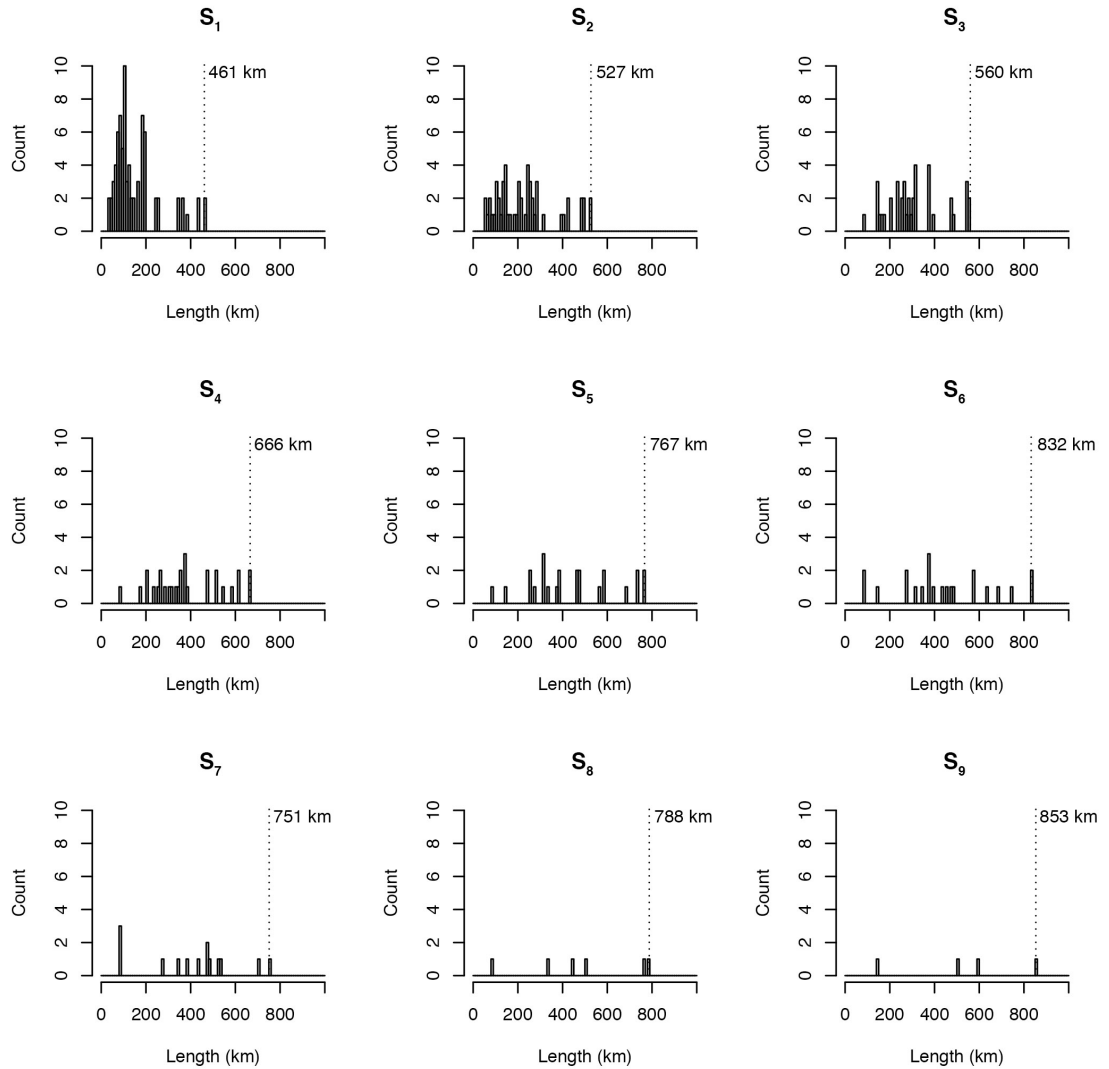


Figure A2: Rupture cascade length distribution at different iterations of the algorithm (case $\Delta = 5$ km in which the number of cascades reaches zero after 9 iterations).

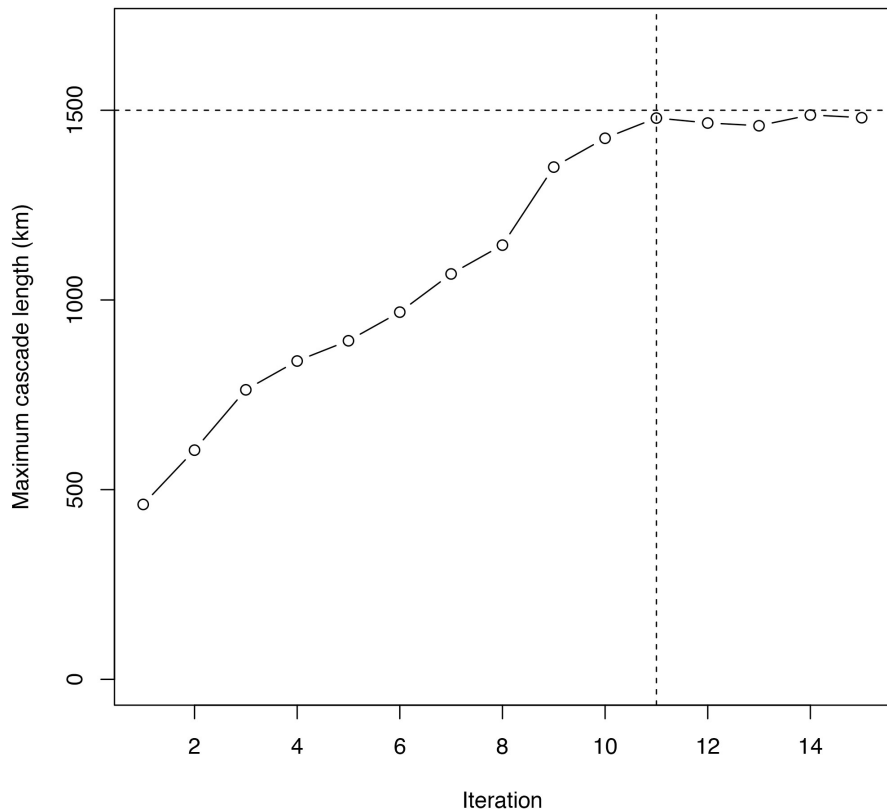


Figure A3: Maximum cascade length L_{max} per iteration. For the case $\Delta = 10$ km, L_{max} reaches a plateau at iteration $i = 11$.